The Role of Shallow Convection over the Tibetan Plateau

YUNYING LI

School of Marine and Atmospheric Sciences, Stony Brook University, Stony Brook, New York, and Nanjing University, Nanjing, China

MINGHUA ZHANG

School of Marine and Atmospheric Sciences, Stony Brook University, Stony Brook, New York, and International Center for Climate and Environment Sciences, Institute of Atmospheric Physics, Chinese Academy of Sciences, Beijing, China

(Manuscript received 15 August 2016, in final form 1 April 2017)

ABSTRACT

Cumulus (Cu) from shallow convection is one of the dominant cloud types over the Tibetan Plateau (TP) in the summer according to *CloudSat–CALIPSO* observations. Its thermodynamic effects on the atmospheric environment and impacts on the large-scale atmospheric circulation are studied in this paper using the Community Atmospheric Model, version 5.3 (CAM5.3). It is found that the model can reasonably simulate the unique distribution of diabatic heating and Cu over the TP. Shallow convection provides the dominant diabatic heating and drying to the lower and middle atmosphere over the TP. A sensitivity experiment indicates that without Cu over the TP, large-scale condensation and stratiform clouds would increase dramatically, which induces enhanced low-level wind and moisture convergence toward the TP, resulting in significantly enhanced monsoon circulation with remote impact on the areas far beyond the TP. Cu therefore acts as a safety valve to modulate the atmospheric environment that prevents the formation of superclusters of stratiform clouds and precipitation over the TP.

1. Introduction

Shallow cumulus convection has an average daytime occurrence frequency of about 30% in the tropics and northern midlatitudes. It plays an important role in determining the fraction of low clouds in the tropics and subtropics (van Stratum et al. 2014). Over the Tibetan Plateau (TP), cumulus (Cu; including shallow cumuli and cumulus congestus) is one of the dominant cloud types in the summer. The frequency of Cu events, defined as Cu occurring within 50-km segments, is 54% over the TP in the summer, which is much larger than in its surrounding regions (Li and Zhang 2016). Cu transports heat and moisture near the surface to the free atmosphere (e.g., Wang and Zhang 2014), causing ventilation of the planet boundary layer (PBL).

Previous studies have identified several roles of shallow cumulus convection in the maintenance of the atmospheric environment: It can evaporate condensates in stratocumulus clouds, thereby impacting large-scale circulation (de Szoeke et al. 2006). Cu entrains warm dry air from the free atmosphere into the boundary layer and weakens the inversion (de Szoeke et al. 2006), thereby impacting the diurnal cycle of the atmospheric boundary layer, which is an important issue for climate simulation (Wilson and Mitchell 1986). Cu may also be a leading factor in determining the cloud–climate feedback (Bony et al. 2004; Bony and Dufresne 2005). Studies have shown that disabling the shallow convection parameterization in atmospheric models would unrealistically increase the stratiform cloud amount, reduce the surface evaporation, and reduce the free-tropospheric humidity (McCaa and Bretherton 2004; Wang et al. 2004; von Salzen et al. 2005; Zhu and Bretherton 2004).

The purpose of this study is to investigate the specific role of the ubiquitous shallow convection over the TP in the maintenance of the atmospheric environment both locally and remotely. We will first evaluate the Community Atmospheric Model, version 5.3 (CAM5.3),

Corresponding author: Prof. Minghua Zhang, minghua.zhang@stonybrook.edu

DOI: 10.1175/JCLI-D-16-0599.1

© 2017 American Meteorological Society. For information regarding reuse of this content and general copyright information, consult the AMS Copyright Policy (www.ametsoc.org/PUBSReuseLicenses).

in simulating the atmospheric circulation, diabatic heating, and clouds over the TP. We will then use the model to investigate the role of shallow convection over the TP. The paper is organized as follows. Section 2 is a brief introduction of data and model experiment design. Section 3 uses the unique active remote sensing capabilities of the satellites to evaluate the representation of Cu in a climate model. Section 4 is an analysis of relative thermodynamical effects of Cu compared to those of other cloud types. It also studies the impact of Cu on large-scale circulation in a model sensitivity experiment. Section 5 contains a summary.

2. Data and model experiment design

a. Data

The Cu in the products of *CloudSat* (Stephens et al. 2008) and the *Cloud–Aerosol Lidar and Infrared Pathfinder Satellite Observations* (*CALIPSO*) (Winker et al. 2009) is defined as isolated clouds with base height at 0–3 km above the ground, horizontal scale of 1–10 km, vertical extent of shallow or moderate, and a liquid water path larger than zero, with or without drizzle and snow. Cumulus cloud fraction observation for model evaluation is from *CloudSat* and *CALIPSO* data from June 2006 to December 2010. The combined radar and lidar 2B-CLDCLASS–lidar level 2 product (Sassen and Wang 2008, 2012) is used in this study as the primary dataset, the Cloud Profiling Radar (CPR) product 2B-CLDCLASS (Wang and Sassen 2007) is used as a supplement when no lidar data are available, which includes the year 2006 and 19.7% of all cases in years 2007–10. In this study, the orbit information is spatially and temporally aggregated to monthly gridded data by merging all profiles in one month in a given 1° × 1° grid size to match the model resolution. The vertical resolution of 0.24 km in the original data is preserved. The cloud fraction in each of the 80 layers from the sea surface to an altitude of 19.2 km is calculated as the ratio of the profile number of a certain cloud type to the total profile number in all grid boxes. The original data contain eight cloud types, but only Cu is studied in this work. The detailed description of this gridded monthly dataset and uncertainties can be found in Li and Zhang (2016).

Because Cu over the TP is most abundant in the summer, unless otherwise specified, the observations in this study are for June–August (JJA) averaged from 2006 to 2010. The latitude of 35°N is selected as a typical zonal cross section to represent the main body of the TP. The cross sections in all figures are averaged over about 1° centered along this latitude unless otherwise noted.

ERA-Interim data (Dee et al. 2011) with a corresponding 1° × 1° resolution from June 2006 to December 2010 are used to describe the observed large-scale atmospheric circulation. Monthly data are used to calculate the climatology, while daily data are used to calculate apparent heat source and apparent moisture sink.

b. Model and experiment design

A numerical experiment is performed by using CAM5.3 of the Community Earth System Model (CESM), version 1.2.2 (http://www.cesm.ucar.edu/) (Gent et al. 2011). The finite-volume dynamical core with a resolution of 0.9° × 1.25°_gx1v6 (a 1° atmosphere/land grid with a nominal 1° ocean/ice grid using the gx1v6 ocean mask) is used to approximately match the gridded *CloudSat–CALIPSO* data. For physical processes, the model uses the Zhang and McFarlane (1995) deep convection scheme and the University of Washington (UW) shallow convection scheme (Park and Bretherton 2009), the prognostic double-moment microphysics of Morrison and Gettelman (2008) with ice supersaturation (Gettelman et al. 2010) and diagnostic precipitation at each model level, and a diagnostic cloud fraction scheme (Park et al. 2014). The simulation uses the standard CAM5.3 settings (Neale et al. 2012), including sea surface temperature, solar constant, and the concentration of main greenhouse gases. The model was run continuously from 1 January 2006 to 31 December 2010 to match the observation period, and the results in JJA of 2006–10 were analyzed.

To evaluate the role of Cu bearing shallow convection in the atmosphere, a sensitivity experiment is designed, in which over the TP region where topography is above 2 km, the Cu cloud fraction as well as the temperature, water vapor, and all cloud hydrometeor tendencies from the UW shallow convection parameterization are removed. The effect of this sensitivity experiment is that Cu is disabled in the TP region.

For comparison between model results and the satellite observations, the cloud fractions in the native vertical model coordinate are converted to those in altitude coordinates according to the geopotential height (HGT) in the model.

We note that Cu in satellite observations are not defined exactly the same as the shallow convective clouds in the model. There is no top height limitation for Cu in the *CloudSat–CALIPSO* product; sometimes it occurs in multiple levels or includes congestus. We constructed the cloud statistics using 4 years of data and found that, over the TP, the median bottom height is 0.72 km, the median top height is 1.44 km, and the median horizontal scale is 2.2 km. The occurrence frequency of Cu whose top height relative to the surface is higher than 3 km is only 5%. Therefore, Cu in the product mainly denotes

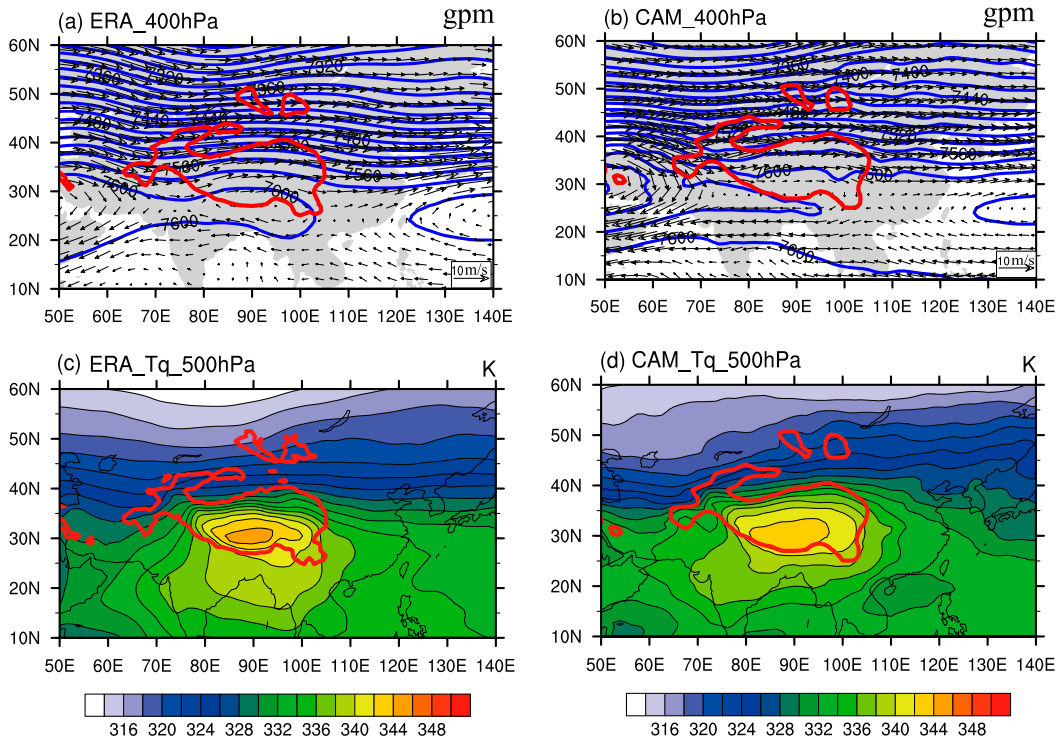

FIG. 1. Geopotential height (blue solid lines) and wind (vectors) at 400 hPa derived from (a) ERA-Interim and (b) CAM5.3. Moist static energy temperature at 500 hPa derived from (c) ERA-Interim and (d) CAM5.3. The red solid lines denote the 2-km topography height referred to as TP in ERA-Interim and CAM5.3, respectively (hereinafter the same meaning in all figures).

shallow cumuli. In the model, shallow cumulus is calculated from the convective mass flux from the shallow convection scheme. It is not a direct output of the standard model diagnostics, and we extracted the field from the model code. Shallow and deep convections in the model differ in that the deep convection requires convective available potential energy (CAPE) larger than the threshold of 70 J kg^{-1}, while the shallow convection does not require a minimum value of CAPE; the plumes in shallow convection entrain less than those in deep convection. As a result, cloud-top height from shallow convection is generally lower than that from deep convection. We found that the top height of shallow cumulus is generally lower than 3 km while that from deep convection reaches a higher altitude. Therefore, the Cu in satellite data can represent the clouds produced by shallow convections in the model.

The CPR surface echo contaminates the first three or four bins (~1.0 km) above the surface. Small Cu (e.g., fair-weather Cu) is likely underrepresented in the *CloudSat* data near the surface. Many warm Cu also lack hydrometeors of sufficient size to enable millimeter-wave radar detection (Sassen and Wang 2008). These uncertainties are not expected to affect the main conclusions of this study.

3. Evaluation of CAM5.3 over the TP

a. Large-scale atmospheric conditions and Cu fraction

Figures 1a and 1b compare the geopotential height and wind fields between ERA-Interim and CAM5.3 at the 400-hPa level, which corresponds to the free troposphere in the region surrounding the TP. The model reasonably captures the large-scale dynamic circulation that includes the splitting westerly toward the TP, the easterly south of TP, and a weak trough along the coast of east China. The model also captures a relatively reasonable South Asia high at high levels over the TP (not shown).

Li and Zhang (2016) used satellite data and reanalysis products to show that the ubiquitous Cu over the TP is mainly caused by the higher air temperature and larger relative humidity on the surface. This environmental condition can be conveniently represented by using the moist static energy, expressed using the moist static energy temperature T_q as follows:

$$T_q = T + \frac{g}{C_p} z + \frac{Lq}{C_p}, \tag{1}$$

where T is the air temperature, z is geopotential height, g is gravity acceleration, q is specific humidity, C_p is the

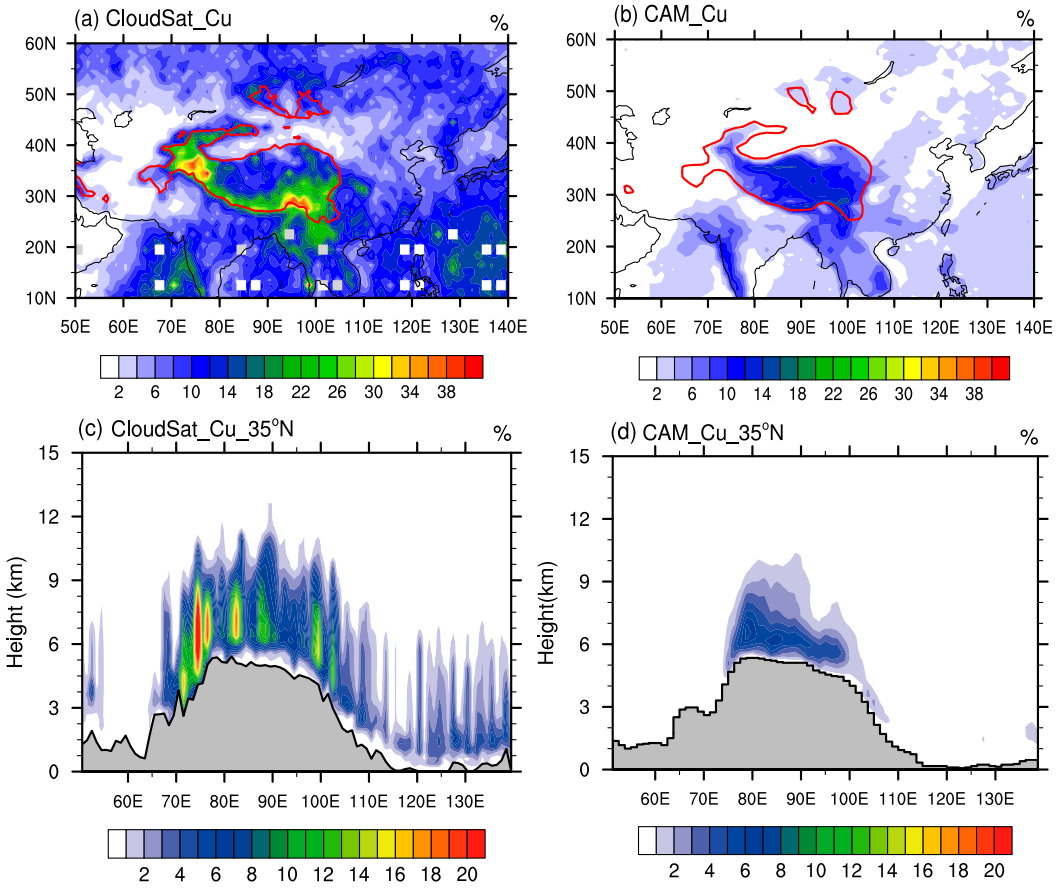

FIG. 2. Spatial distributions of cumulus cloud fraction derived from (a) *CloudSat–CALIPSO* and (b) CAM5.3. Vertical distributions of cumulus cloud fraction along 35°N derived from (c) *CloudSat–CALIPSO* and (d) CAM5.3. White squares in (a) mean missing data. The gray areas denote true and model topography in (c) and (d), respectively.

specific heat at constant pressure, and L is latent heat of condensation. The spatial distributions of T_q at 500 hPa in JJA in ERA-Interim and CAM5.3 are shown in Figs. 1c and 1d, respectively. Because the average surface elevation of TP is higher than 4 km, the 500-hPa level can be used to represent atmospheric conditions near the surface of the TP that have the largest impact on shallow convection. It can be seen that T_q is higher over the TP than surrounding regions by 10 K or more, in both ERA-Interim and CAM5.3. The maximum value of T_q in CAM5.3 is about 2 K smaller than in ERA-Interim, but the model captured the characteristics of larger T_q over the TP.

The spatial distribution of Cu in JJA in the *CloudSat–CALIPSO* data is illustrated in Fig. 2a, where the TP is outlined by the 2-km topography height. The Cu fraction over the TP is larger than over its surrounding areas, with the maximum belt along the southern steep slope of the TP. Although the cloud cover in the model (Fig. 2b) is smaller than observations, and the maximum cloud belt along the southern steep slope is not as clear as that in observations, the main characteristics of the Cu spatial distribution over the TP are reproduced in the model, except in the region of the southern steep slope. It is possible that the overly active deep convection on the steep southern flank of the plateau causes the negative bias of the shallow convection in the model.

We next turn to examine the vertical distribution of Cu along 35°N in observations (Fig. 2c) and in the simulation (Fig. 2d). The model simulated maximum Cu over the TP with similar vertical extent as in observations despite the cloud fraction in the model being smaller overall than in observations. The simulated depth is generally less than 3 km, while observed Cu can reach 5 km. As mentioned before, the Cu definitions in the observations and model are not exactly the same, so exact consistency of the Cu fraction is not expected. In addition, the smaller T_q in the model than observations shown in Figs. 1c and 1d may also be a reason that leads to the relatively lower cloud-top height in the model than in observations. The ability of the model in simulating Cu over the TP is in sharp contrast to that in eastern China, where little Cu is simulated relative to

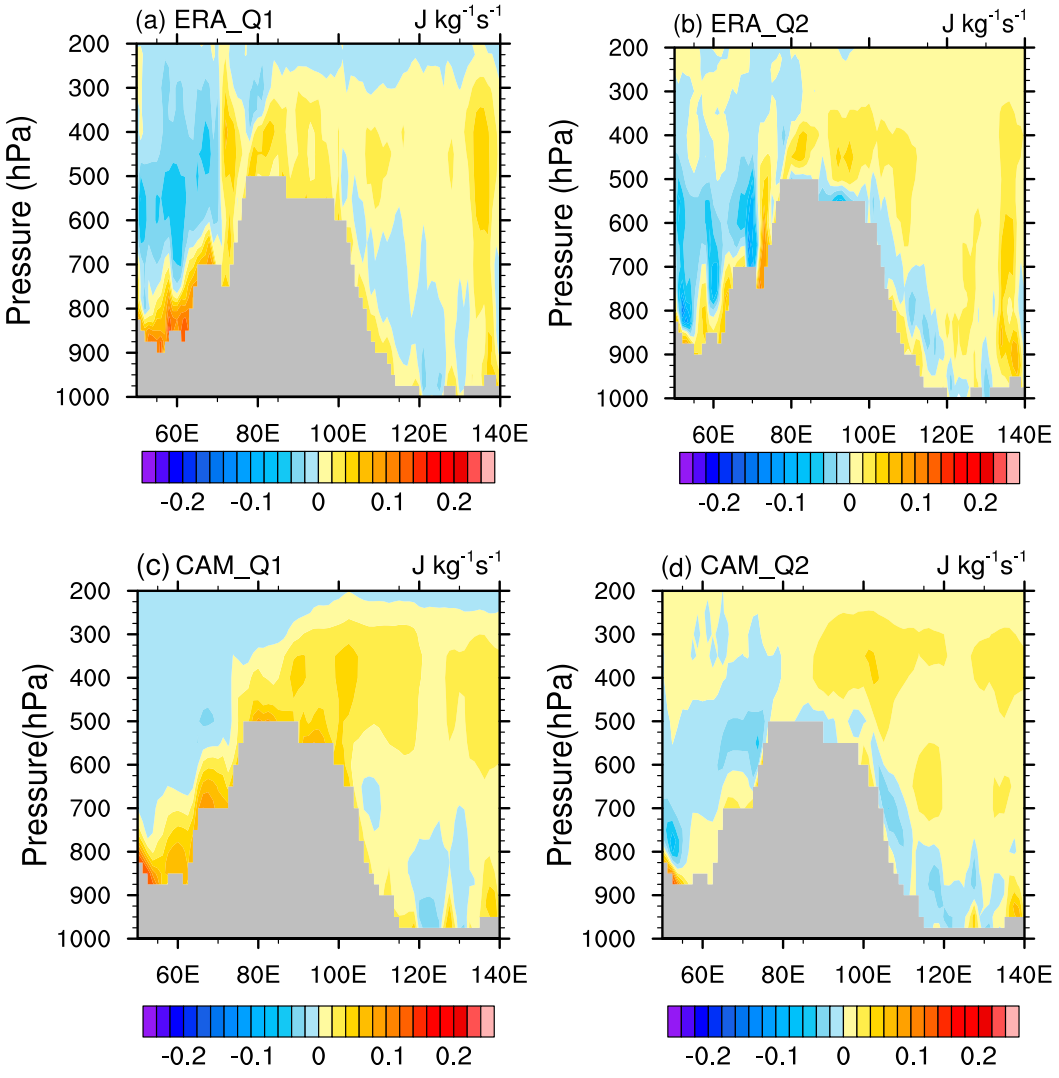

FIG. 3. The vertical distribution of Q_1 along 35°N derived from (a) ERA-Interim and (c) CAM5.3. The vertical distribution of Q_2 along 35°N derived from (b) ERA-Interim and (d) CAM5.3. The positive (negative) values in Q_1 indicate the increase (decrease) of temperature; the positive (negative) values in Q_2 indicate the decrease (increase) of the water vapor.

observations, which is as a result of the overly active deep convection scheme in eastern China in the model.

b. Apparent heat source and water vapor sink

Following Yanai et al. (1973), the atmospheric diabatic heating and moisture can be diagnosed by using the apparent heat Q_1 and apparent moisture sink Q_2. The apparent heat can be calculated as

$$Q_1 = C_p\left[\frac{\partial T}{\partial t} + \mathbf{V}\cdot\nabla T + \left(\frac{p}{p_0}\right)^k \omega\frac{\partial\theta}{\partial p}\right], \tag{2}$$

where T is temperature, t is time, $\mathbf{V}$ is horizontal velocity vector, p is air pressure, ω is the pressure vertical velocity (Pa s^{-1}), θ is the potential temperature, p_0 is the reference air pressure 1000 hPa, and k is a constant of 0.286. The apparent moisture sink can be calculated as

$$Q_2 = -L\left(\frac{\partial q}{\partial t} + \mathbf{V}\cdot\nabla q + \omega\frac{\partial q}{\partial p}\right), \tag{3}$$

where q is specific humidity and L is latent heat of condensation.

The Q_1 and Q_2 in each vertical level are calculated using daily ERA-Interim data. The vertical distributions of Q_1 and Q_2 along 35°N are shown in Figs. 3a and 3b, respectively. Above the level of 500 hPa over the TP, Q_1 is positive in the lower and middle troposphere; Q_2 is negative in the immediate surface and is positive above it. The near-surface distributions of Q_1 and Q_2 are consistent with

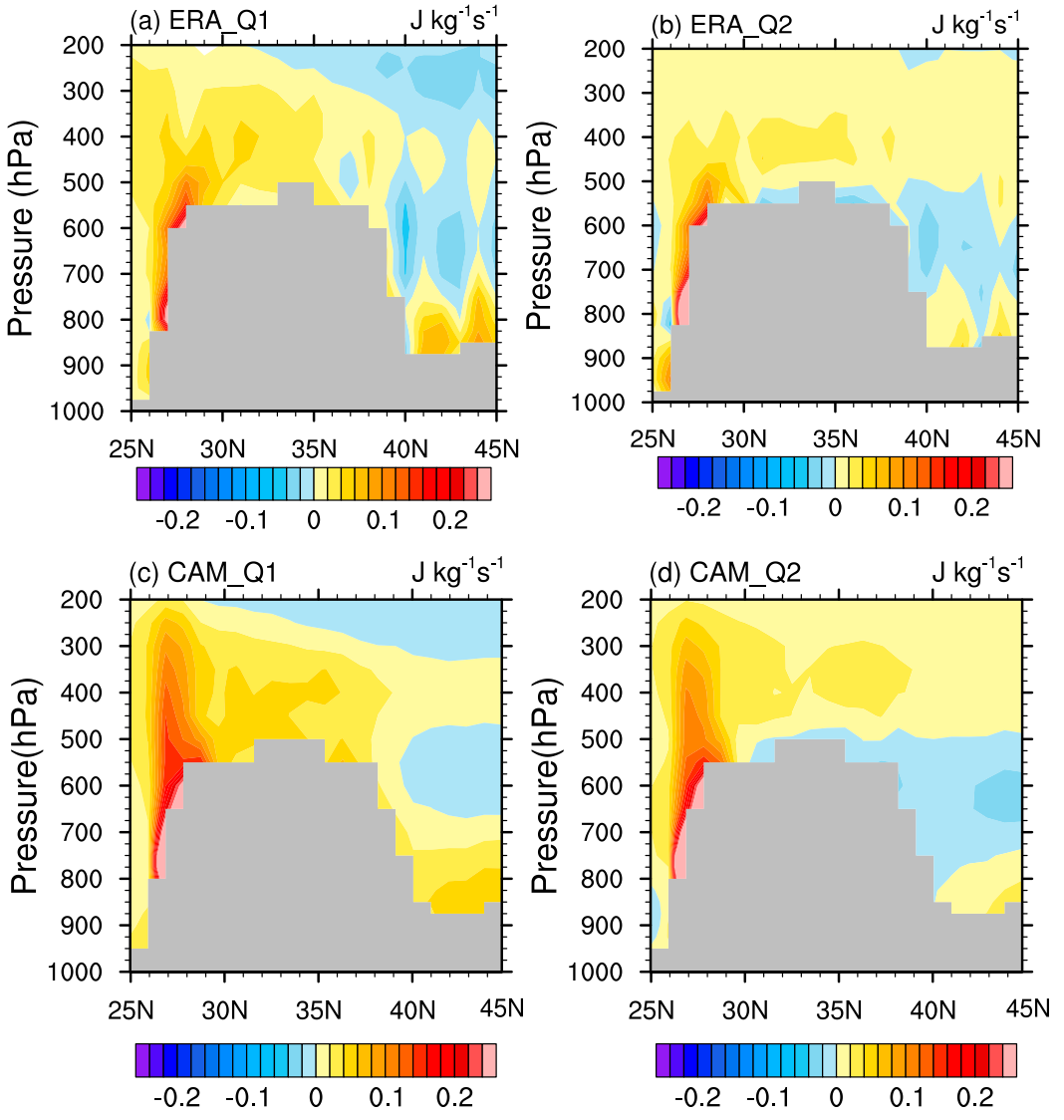

FIG. 4. As in Fig. 3, but for values along 90°E.

positive surface sensible and latent heat fluxes that warm and moisten the atmospheric boundary layer. The low- and midtropospheric distributions are consistent with latent heating and condensation of water vapor.

In the model, Q_1 and Q_2 (shown in Figs. 3c,d, respectively) are calculated directly from the temperature and specific humidity tendencies in the physical parameterizations. Figure 3c shows that Q_1 over the TP in the model is positive in the lower and middle troposphere, similar to the observations. Figure 3d shows that Q_2 is also similar to observations in that it is mostly negative near the immediate surface and is positive above it. The distributions of Q_1 and Q_2 are qualitatively similar between the model and observations in terms of the signs and order of magnitude. Quantitatively the values in the model and observation are different, with the model generally showing larger values. This is consistent with model biases of overestimated precipitation over the TP that are common in many climate models, including CAM5.3 (e.g., Su et al. 2013). For the present study, in observation, the occurrence frequency of shallow convection Cu over the TP is 18%, whereas deep convection is only 3% (Li and Zhang 2016, their Fig. 2). The model also simulated much smaller amounts of deep convective clouds than Cu and little temperature and moisture tendency from the deep convection scheme. Biases in precipitation can remotely impact the shallow convection. For our purpose, however, since we are concerned with the qualitative role of shallow convection, we consider CAM5.3 to have reasonably reproduced the observed

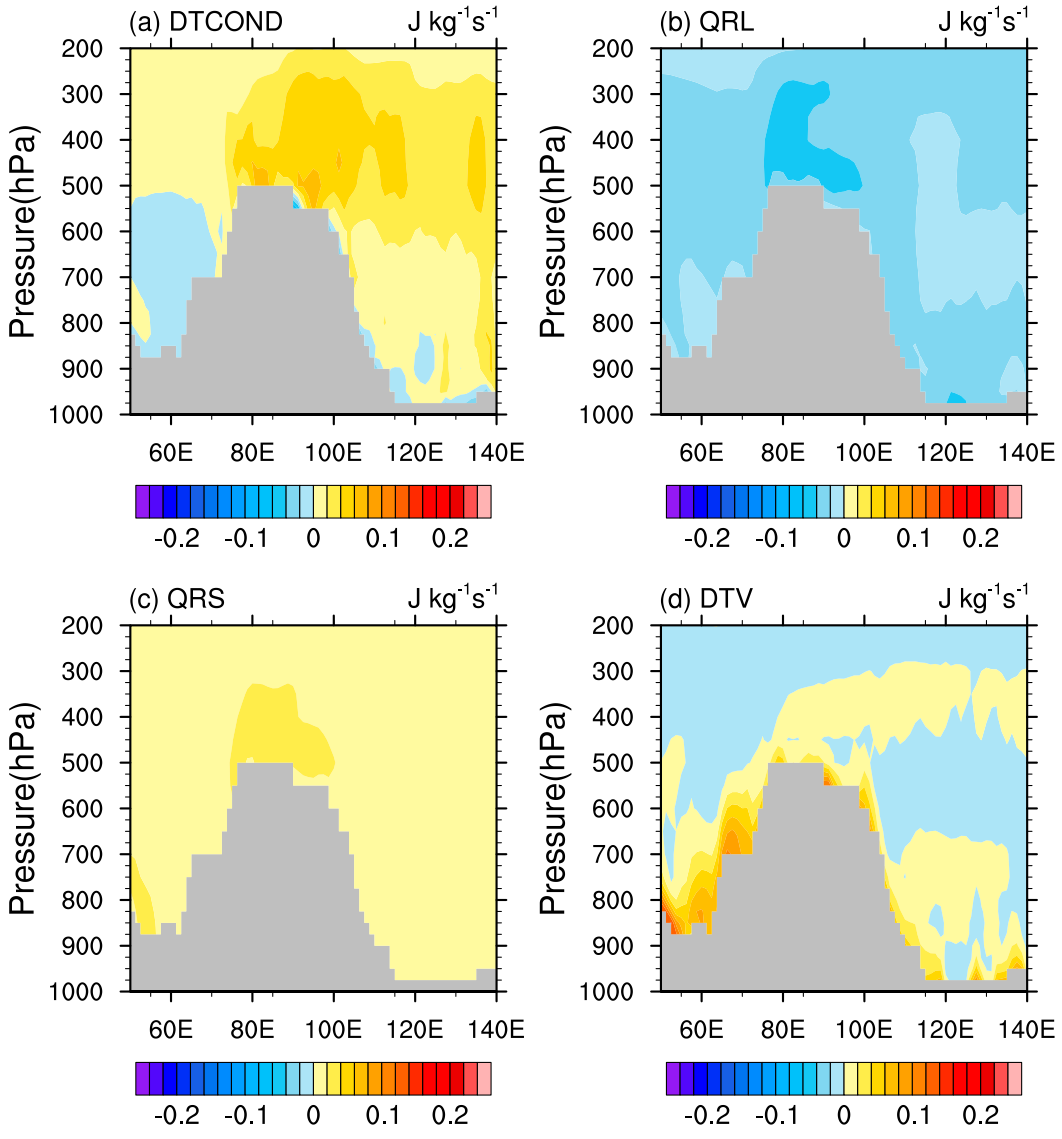

FIG. 5. The vertical distribution of the apparent heat source component along 35°N derived from (a) DTCOND, (b) QRL, (c) QRS, and (d) DTV. The positive (negative) values indicate temperature increase (decrease) in the atmosphere.

dynamic and thermodynamic atmospheric environment and the Cu occurrence over the TP. As will be shown later, our results on the role of shallow convection are relevant to the understanding of the precipitation over TP. The comparison of Q_1 and Q_2 between the model simulations and ERA-Interim along a north–south cross section at 90°E is qualitatively similar to that along the zonal section. This is shown in Fig. 4.

4. The role of shallow convection over the TP

a. *The thermodynamic effect*

The modeled Q_1 allows us to attribute the large-scale diabatic heating into different physical processes that consist of diabatic heating from moist physics (DTCOND), solar radiative heating (QRS), longwave radiative cooling (QRL), and turbulent vertical transport of heat (DTV):

$$Q_1 = \left(\frac{\partial T}{\partial t}\right)_{\mathrm{DTCOND}} + \left(\frac{\partial T}{\partial t}\right)_{\mathrm{QRS}} + \left(\frac{\partial T}{\partial t}\right)_{\mathrm{QRL}} + \left(\frac{\partial T}{\partial t}\right)_{\mathrm{DTV}}. \tag{4}$$

Figures 5a–d show each of the terms on the right-hand side of Eq. (4). The moist physics term $(\partial T/\partial t)_{\mathrm{DTCOND}}$ contributes the most to the diabatic heating, much larger than the atmospheric absorption of solar radiation $(\partial T/\partial t)_{\mathrm{QRS}}$, except near the surface, where the turbulent heat transport term $(\partial T/\partial t)_{\mathrm{DTV}}$ is dominant. Over

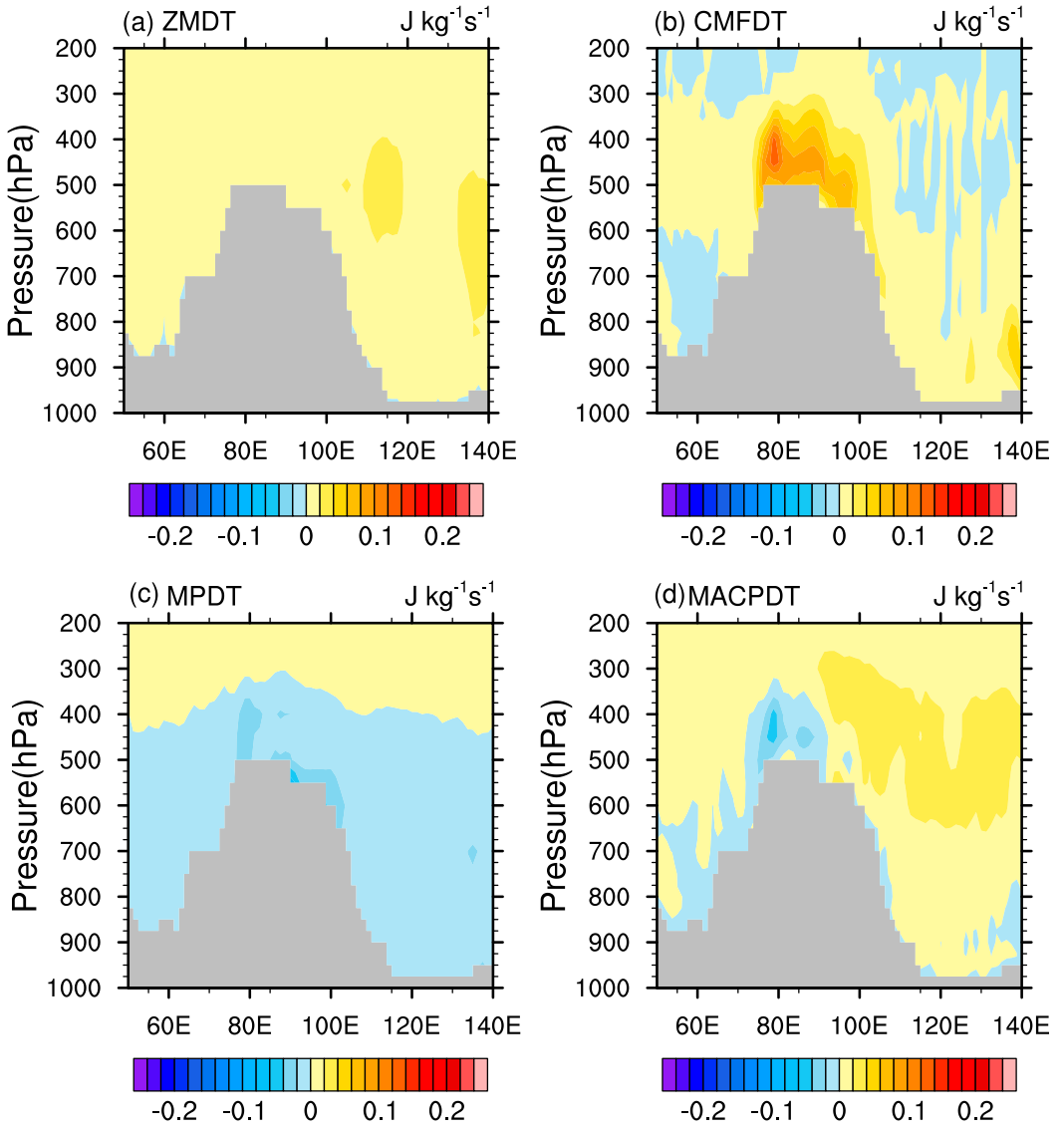

FIG. 6. The vertical distribution of the apparent heat source component along 35°N derived from (a) ZMDT, (b) CMFDT, (c) MPDT, and (d) MACPDT. The positive (negative) values indicate temperature increase (decrease) in the atmosphere.

the TP, the magnitude of the longwave radiative cooling term $(\partial T/\partial t)_{\mathrm{QRL}}$ is as large as the shortwave heating even in the summer. This is presumably because the atmosphere over the TP is warmer and moister than most other places at the same latitude and same altitude. Overall, the atmosphere over the TP is a heat source, consistent with many previous studies (e.g., Wu et al. 2015).

The diabatic heating from the moist physics $(\partial T/\partial t)_{\mathrm{DTCOND}}$ can be further attributed to contributions from deep convection (ZMDT), shallow convection (CMFDT), stratiform microphysical physical processes (MPDT), and stratiform macrophysical processes (MACPDT), written as the following with several minor terms neglected:

$$\left(\frac{\partial T}{\partial t}\right)_{\mathrm{DTCOND}} \approx \left(\frac{\partial T}{\partial t}\right)_{\mathrm{ZMDT}} + \left(\frac{\partial T}{\partial t}\right)_{\mathrm{CMFDT}} + \left(\frac{\partial T}{\partial t}\right)_{\mathrm{MPDT}} + \left(\frac{\partial T}{\partial t}\right)_{\mathrm{MACPDT}}. \quad (5)$$

In CAM5.3, MACPDT represents condensational heating/evaporation associated with the change of stratiform cloud amount (Zhang et al. 2003); MPDT represents additional heating/cooling from condensation/evaporation of rain, snow, and phase change of cloud particles between

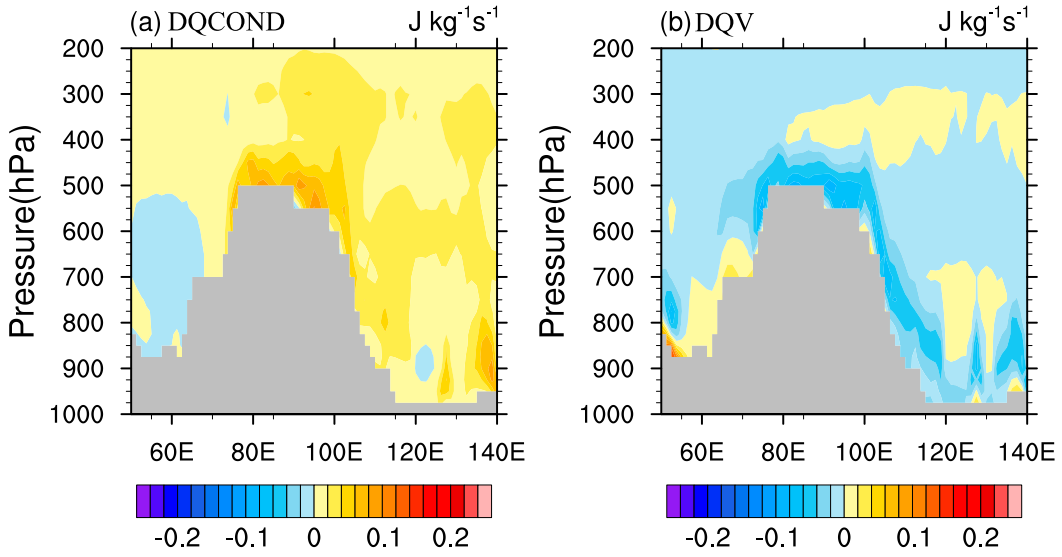

FIG. 7. The vertical distribution of the apparent water vapor sink component along 35°N derived from (a) DQCOND and (b) DQV. The positive (negative) values indicate water vapor decrease (increase) in the atmosphere.

liquid and solid. Figures 6a–d show each of the terms on the right-hand side of Eq. (5). The most striking feature is the dominance of the shallow convection term $(\partial T/\partial t)_{\mathrm{CMFDT}}$ over the TP that is positive throughout the lower and middle troposphere. Second to the shallow convection is the contribution of large-scale stratiform evaporative cooling in the lower troposphere and condensational heating above it from the $(\partial T/\partial t)_{\mathrm{MACPDT}}$ term.

The combined information in Figs. 5 and 6 suggests that the atmosphere near the surface over the TP is heated by turbulent transport as a result of surface sensible heat flux, while the lower and middle troposphere is heated by shallow convection, whose energy can come from both the surface buoyancy flux and boundary layer air moist static energy. Evaporative cooling of falling rain from shallow convection offsets the lower-tropospheric warming to some extent.

A similar analysis is performed for the apparent moisture sink, written as follows:

$$Q_2 = \left[-L\left(\frac{\partial q}{\partial t}\right)\right]_{\mathrm{DQCOND}} + \left[-L\left(\frac{\partial q}{\partial t}\right)\right]_{\mathrm{DQV}}, \quad (6)$$

where the first and second terms represent contributions of moist physics (DQCOND) and vertical transport (DQV), respectively. The two terms are shown in Fig. 7. Positive values represent moisture sink, while negative values represent moisture source. It is seen that the moist physics removes water vapor from the atmosphere, while the turbulent transport moistens the boundary layer from surface latent heat flux.

Similar to $(\partial T/\partial t)_{\mathrm{DTCOND}}$ as for in Q_1, the moist physics term $(\partial q/\partial t)_{\mathrm{DQCOND}}$ is also further decomposed into four terms, as follows:

$$\left(\frac{\partial q}{\partial t}\right)_{\mathrm{DQCOND}} \approx \left(\frac{\partial q}{\partial t}\right)_{\mathrm{ZMDQ}} + \left(\frac{\partial q}{\partial t}\right)_{\mathrm{CMFDQ}} + \left(\frac{\partial q}{\partial t}\right)_{\mathrm{MPDQ}} + \left(\frac{\partial q}{\partial t}\right)_{\mathrm{MACPDQ}}; \quad (7)$$

they represent contributions from deep convection (ZMDQ), shallow convection (CMFDQ), stratiform microphysical physical processes (MPDQ), and stratiform macrophysical processes (MACPDQ). Over the TP, the dominant contribution to Q_2 is from the shallow convection term $(\partial q/\partial t)_{\mathrm{CMFDQ}}$. The contribution of large-scale stratiform evaporation $(\partial q/\partial t)_{\mathrm{MACPDQ}}$ is the second largest. Other terms are negligible in the moist physics tendency.

Shallow convection can dry the atmosphere in two ways (e.g., Zhang et al. 2013). The first is through condensation of water vapor; the second is through subgrid-scale vertical exchange of water vapor by the convective plumes. The strong similarity between Q_1 and Q_2 from the shallow convection in Fig. 6b and Fig. 8b indicates that the drying is primarily caused by condensation. The Q_2 distributions in Figs. 7 and 8 suggest that there is a source of moisture in the boundary layer due to surface latent heat flux and a sink of moisture in the troposphere due to condensation in Cu.

The role of shallow convection over the TP can be therefore summarized to warm and dry the lower and middle troposphere through condensation, which are the dominant diabatic heating and moisture sink terms

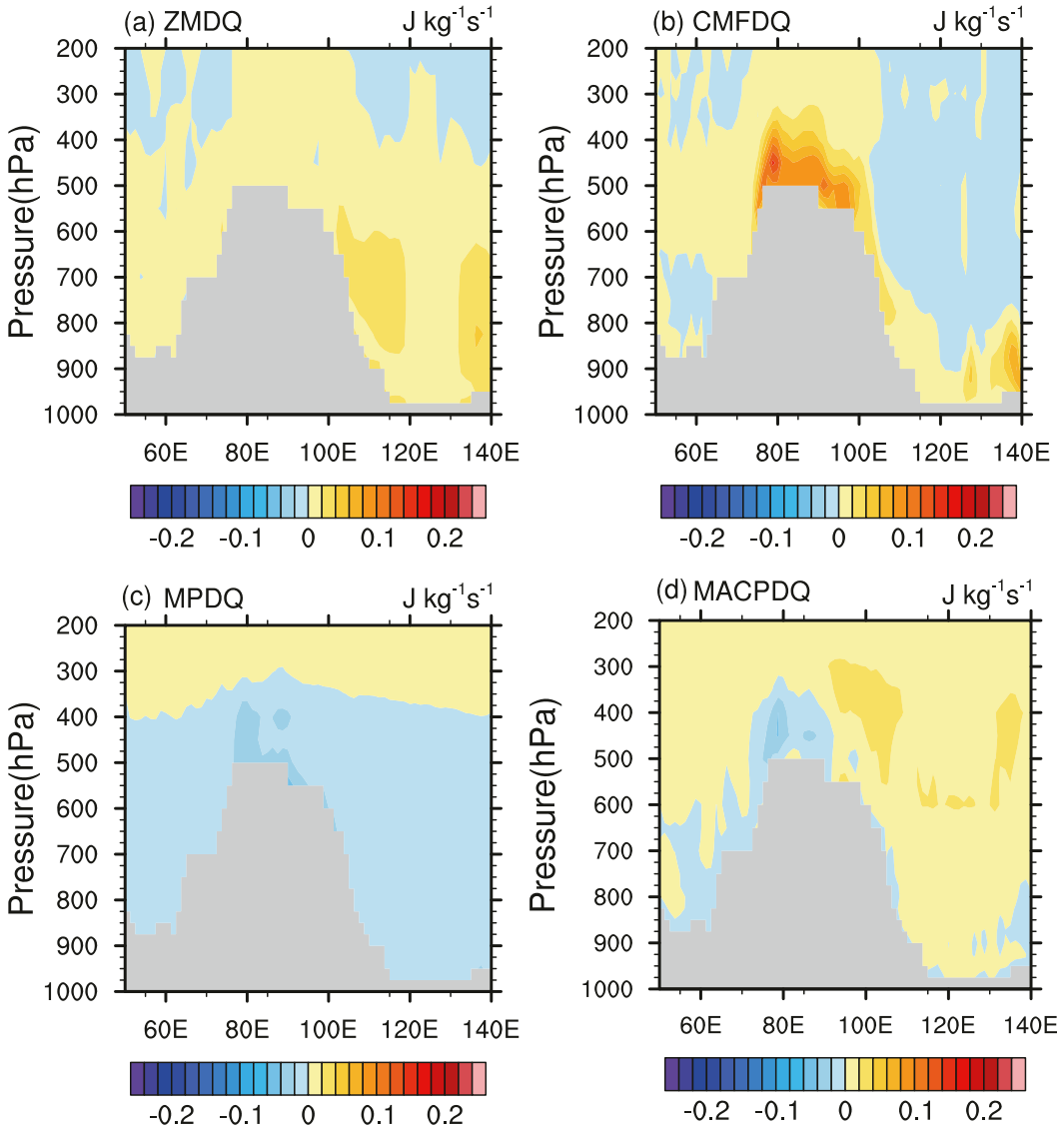

FIG. 8. The vertical distribution of the apparent water vapor sink component along 35°N derived from (a) ZMDQ, (b) CMFDQ, (c) MPDQ, and (d) MACPDQ. The positive (negative) values indicate water vapor decrease (increase) in the atmosphere.

over the TP. The shallow convection derives its moisture and energy from the boundary layer and the surface.

b. *The impacts of shallow convection on large-scale circulation*

We next investigate the role of shallow convection over the TP in the maintenance of the large-scale atmospheric circulation. If there were no shallow convection over the TP, what would the circulation look like? A model sensitivity experiment is carried out to answer this question. In the sensitivity experiment, the shallow convection over the TP, as well as the temperature and water vapor tendencies derived from the UW convection parameterization were removed, which means the shallow convection parameterization is effectively disabled over the TP region.

As shown in Fig. 9, without shallow convection over the TP, the stratiform cloud fraction is found to increase dramatically when compared to that in the control run (Fig. 9b vs Fig. 9a). The difference in the stratiform cloud fraction between the sensitivity experiment and control run (Fig. 9c) occurs both over the TP region and in a passage of the South Asian summer monsoon, passing the 95% significant test (Fig. 9c, hatched), with the maximum difference up to 50% in the main body of the TP.

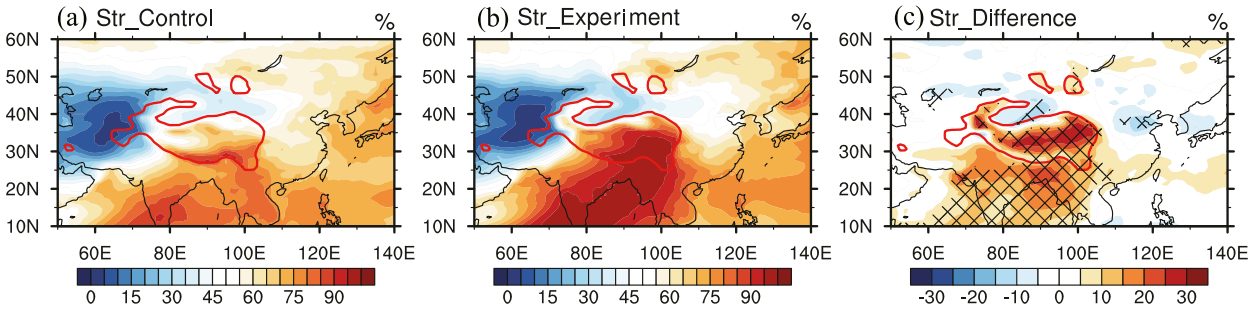

FIG. 9. Stratiform cloud fractions derived from the (a) control run and (b) sensitivity experiment. (c) The difference of stratiform cloud fraction between model experiment and control run. The hatched areas in (c) are significant at the 95% level.

This increase of stratiform clouds when shallow convection is removed can be explained as follows: without the heating and drying effects of shallow convection in the lower and middle troposphere, the temperature would decrease, and the specific humidity would increase, both of which will lead to increase of relative humidity and thus more large-scale condensation and stratiform clouds.

The sign of the apparent heat component from the stratiform macrophysical processes turns from negative to positive, indicating changes from evaporate cooling to condensation warming as a result of large quantities of stratiform clouds (cf. Fig. 10a vs Fig. 6d). The sign of apparent moisture sink also turns from negative to positive, indicating changes from water vapor source to water vapor sink (cf. Fig. 10b vs Fig. 8d). This change of latent heating is associated with large responses in the atmospheric circulation beyond the TP. Figure 11a shows the distribution of the difference in sea level pressure, with the hatched area denoting statistically significant signals. Pressure decreases over much of the Eurasian continent, especially in South Asia, and in the southern Indian Ocean, the mechanism of which is not clear to us. As expected, strong horizontal surface winds converge to the central TP (Fig. 11b, vectors), resulting in larger moisture flux convergence in the central TP and compensation divergence to the north and south of TP (Fig. 11b, shaded). Figure 11b also shows the Asia monsoon circulation in low atmosphere is strengthened significantly.

5. Summary

We have evaluated the ability of CAM5.3 in simulating the dominance of Cu over the TP as observed by satellite measurements. It shows that the model can simulate the much larger presence of Cu over the TP than in its surrounding regions. The model is also able to

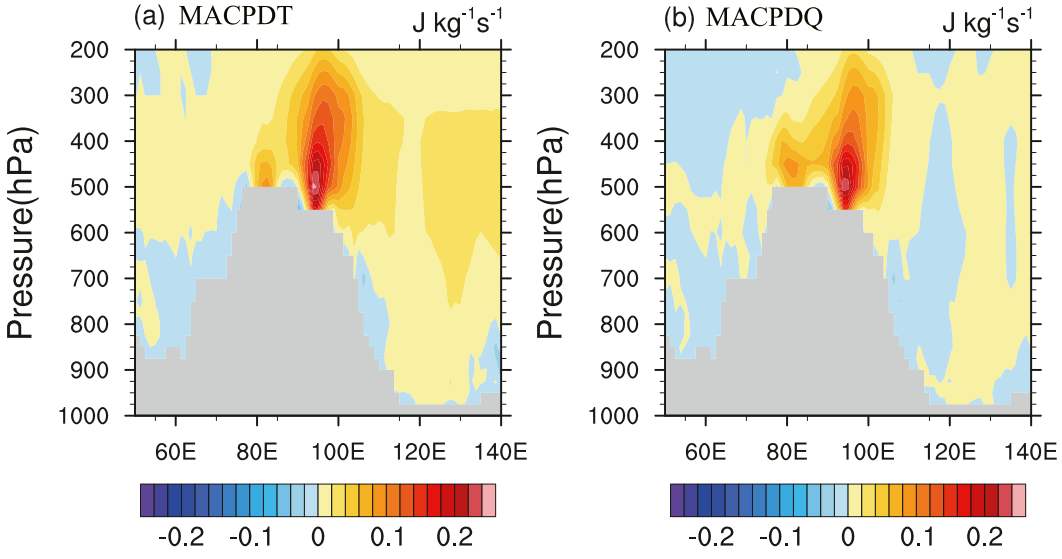

FIG. 10. The vertical distribution of the (a) apparent heat source component and (b) apparent water vapor sink component along 35°N derived from the macro stratiform cloud process in the model sensitivity experiment.

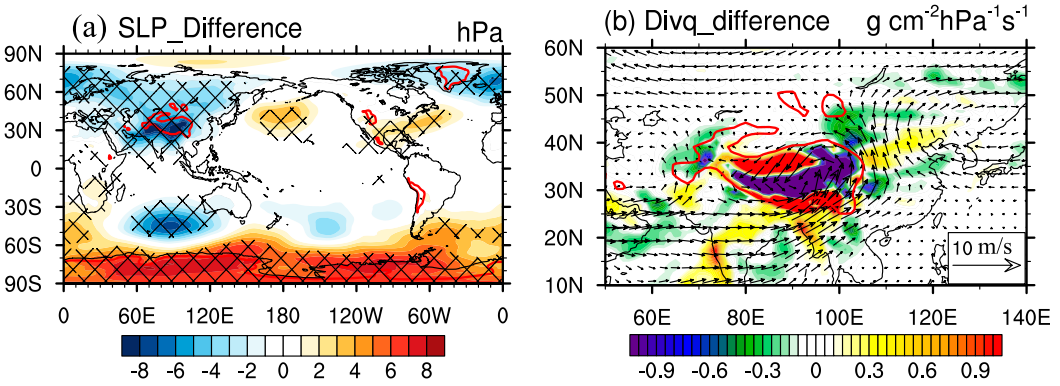

FIG. 11. The difference of (a) sea surface air pressure and (b) moisture flux divergence (shaded) and wind (vector) at 500 hPa between the model sensitivity experiment and control run. The hatched areas in (a) are significant at the 95% level.

reasonably capture the distributions of the apparent diabatic heating and moist sink over the TP when compared with the corresponding diagnostics from ERA-Interim.

CAM5.3 is then used to investigate the role of shallow convection over the TP in the atmosphere. Shallow convection is found to account for the dominant source of diabatic heating in the lower and middle troposphere over the TP, which is caused by latent heating associated with Cu. Shallow convection also dries the atmosphere in the lower and middle troposphere. When shallow convection over the TP is removed, the large-scale stratiform condensation increases dramatically, which leads to a strengthened Asian monsoon and more moisture transport into the TP region, with impacts far beyond TP. The ubiquitous presence of Cu and shallow convection over the TP therefore plays the role of ventilating the boundary layer, drying and warming the lower troposphere, and preventing the atmosphere over the TP from reaching large-scale saturation that would otherwise induce a stronger monsoon and more moisture transport to the TP. Shallow convection over the TP therefore plays a key role in the maintenance of the atmospheric circulation and monsoon system in the present climate. Conducting ensemble simulations to further confirm our finding is desirable, but we think the results are robust since the physical mechanism can be explained as reported here.

Acknowledgments. We wish to thank Dr. Wuyin Lin, Linjiong Zhou, and Dr. Xin Xie for valuable discussions and their assistance with the model simulations. This research is supported by the National Natural Science Foundation of China (Grant 41475069), the State Scholarship Fund from China Scholarship Council, the China Special Fund for Public Welfare Industry (meteorology: GYHY 201306068), and the National Major Research High Performance Computing Program of China (Grant 2016YFB02008). Additional support is provided by the Biological and Environmental Research Division in the Office of Sciences of the U.S. Department of Energy (DOE).

REFERENCES

Bony, S., and J. L. Dufresne, 2005: Marine boundary layer clouds at the heart of tropical cloud feedback uncertainties in climate models. *Geophys. Res. Lett.*, **32**, L20806, doi:10.1029/2005GL023851.

——, ——., H. Le Treut, J. J. Morcrette, and C. Senior, 2004: On dynamic and thermodynamic components of cloud changes. *Climate Dyn.*, **22**, 71–86, doi:10.1007/s00382-003-0369-6.

Dee, D. P., and Coauthors, 2011: The ERA-Interim reanalysis: Configuration and performance of the data assimilation systems. *Quart. J. Roy. Meteor. Soc.*, **137**, 553–597, doi:10.1002/qj.828.

de Szoeke, S. P., Y. Wang, S.-P. Xie, and T. Miyama, 2006: Effect of shallow cumulus convection on the eastern Pacific climate in a coupled model. *Geophys. Res. Lett.*, **33**, L17713, doi:10.1029/2006GL026715.

Gent, P. R., and Coauthors, 2011: The Community Climate System Model version 4. *J. Climate*, **24**, 4973–4991, doi:10.1175/2011JCLI4083.1.

Gettelman, A., and Coauthors, 2010: Global simulations of ice nucleation and ice supersaturation with an improved cloud scheme in the Community Atmosphere Model. *J. Geophys. Res.*, **115**, D18216, doi:10.1029/2009JD013797.

Li, Y. Y., and M. H. Zhang, 2016: Cumulus over the Tibetan Plateau in the summer based on *CloudSat–CALIPSO* data. *J. Climate*, **29**, 1219–1230, doi:10.1175/JCLI-D-15-0492.1.

McCaa, J. R., and C. S. Bretherton, 2004: A new parameterization for shallow cumulus convection and its application to marine subtropical cloud-topped boundary layers. Part II: Regional simulations of marine boundary layer clouds. *Mon. Wea. Rev.*, **132**, 883–896, doi:10.1175/1520-0493(2004)132<0883:ANPFSC>2.0.CO;2.

Morrison, H., and A. Gettelman, 2008: A new two-moment bulk stratiform cloud microphysics scheme in the Community Atmosphere Model, version 3 (CAM3). Part I: Description and

numerical tests. *J. Climate*, **21**, 3642–3659, doi:10.1175/2008JCLI2105.1.

Neale, R. B., and Coauthors, 2012: Description of the NCAR Community Atmosphere Model (CAM5.0). NCAR Tech. Note NCAR/TN-486+STR, 274 pp. [Available online at http://www.cesm.ucar.edu/models/cesm1.0/cam/docs/description/cam5_desc.pdf.]

Park, S., and C. S. Bretherton, 2009: The University of Washington shallow convection and moist turbulence schemes and their impact on climate simulations with the Community Atmosphere Model. *J. Climate*, **22**, 3449–3469, doi:10.1175/2008JCLI2557.1.

——, ——, and P. J. Rasch, 2014: Integrating cloud processes in the Community Atmosphere Model, version 5. *J. Climate*, **27**, 6821–6856, doi:10.1175/JCLI-D-14-00087.1.

Sassen, K., and Z. Wang, 2008: Classifying clouds around the globe with the *CloudSat* radar: 1-year of results. *Geophys. Res. Lett.*, **35**, L04805, doi:10.1029/2007GL032591.

——, and ——, 2012: The clouds of the middle troposphere: Composition, radiative impact, and global distribution. *Surv. Geophys.*, **33**, 677–691, doi:10.1007/s10712-011-9163-x.

Stephens, G. L., and Coauthors, 2008: *CloudSat* mission: Performance and early science after the first 5 years of operation. *J. Geophys. Res.*, **113**, D00A18, doi:10.1029/2008JD009982.

Su, F., X. Duan, D. Chen, Z. Hao, and L. Cuo, 2013: Evaluation of the global climate models in the CMIP5 over the Tibetan Plateau. *J. Climate*, **26**, 3187–3208, doi:10.1175/JCLI-D-12-00321.1.

van Stratum, B. J. H., J. Vilá-Guerau de Arellano, C. C. van Heerwaarden, and H. G. Ouwersloot, 2014: Subcloud-layer feedbacks driven by the mass flux of shallow cumulus convection over land. *J. Atmos. Sci.*, **71**, 881–895, doi:10.1175/JAS-D-13-0192.1.

von Salzen, K., N. A. McFarlane, and M. Lazare, 2005: The role of shallow convection in the water and energy cycles of the atmosphere. *Climate Dyn.*, **25**, 671–688, doi:10.1007/s00382-005-0051-2.

Wang, X. C., and M. H. Zhang, 2014: Vertical velocity in shallow convection for different plume types. *J. Adv. Model. Earth Syst.*, **6**, 478–489, doi:10.1002/2014MS000318.

Wang, Y., H. Xu, and S.-P. Xie, 2004: Regional model simulations of marine boundary layer clouds over the southeast Pacific off South America. Part II: Sensitivity experiments. *Mon. Wea. Rev.*, **132**, 2650–2668, doi:10.1175/MWR2812.1.

Wang, Z., and K. Sassen, 2007: Level 2 cloud scenario classification product process description and interface control document, version 5.0. *CloudSat* Project Tech. Rep., 50 pp. [Available online at http://www.cloudsat.cira.colostate.edu/sites/default/files/products/files/2B-CLDCLASS_PDICD.P_R04.20070724.pdf.]

Wilson, C. A., and J. F. B. Mitchell, 1986: Diurnal variation and cloud in a general circulation model. *Quart. J. Roy. Meteor. Soc.*, **112**, 347–369, doi:10.1002/qj.49711247205.

Winker, D. M., M. A. Vaughan, A. H. Omar, Y. Hu, K. A. Powell, Z. Liu, W. H. Hunt, and S. A. Young, 2009: Overview of the *CALIPSO* mission and CALIOP data processing algorithms. *J. Atmos. Oceanic Technol.*, **26**, 2310–2323, doi:10.1175/2009JTECHA1281.1.

Wu, G. X., and Coauthors, 2015: Tibetan Plateau climate dynamics: Recent research progress and outlook. *Natl. Sci. Rev.*, **2**, 100–116, doi:10.1093/nsr/nwu045.

Yanai, M., S. Esbensen, and J. H. Chu, 1973: Determination of bulk properties of tropical cloud clusters from large-scale heat and moisture budgets. *J. Atmos. Sci.*, **30**, 611–627, doi:10.1175/1520-0469(1973)030<0611:DOBPOT>2.0.CO;2.

Zhang, G. J., and N. A. McFarlane, 1995: Sensitivity of climate simulations to the parameterization of cumulus convection in the Canadian Climate Centre general circulation model. *Atmos.–Ocean*, **33**, 407–446, doi:10.1080/07055900.1995.9649539.

Zhang, M. H., W. Lin, C. Bretherton, J. Hack, and P. J. Rasch, 2003: A modified formulation of fractional stratiform condensation rate in the NCAR Community Atmospheric Model (CAM2). *J. Geophys. Res.*, **108**, 4035, doi:10.1029/2002JD002523.

——, and Coauthors, 2013: CGILS: Results from the first phase of an international project to understand the physical mechanisms of low cloud feedbacks in single column models. *J. Adv. Model. Earth Syst.*, **5**, 826–842, doi:10.1002/2013MS000246.

Zhu, P., and C. S. Bretherton, 2004: A simulation study of shallow moist convection and its impact on the atmospheric boundary layer. *Mon. Wea. Rev.*, **132**, 2391–2409, doi:10.1175/1520-0493(2004)132<2391:ASSOSM>2.0.CO;2.